Oxygen-modulated quantum conductance for ultrathin HfO_{2}-based memristive switching devices

Xiaoliang Zhong, Ivan Rungger, Peter Zapol, and Olle Heinonen

Phys. Rev. B **94**, 165160 — Published 24 October 2016

DOI: 10.1103/PhysRevB.94.165160

Oxygen modulated quantum conductance for ultra-thin HfO_2-based memristive switching devices

Xiaoliang Zhong,[1, a)] Ivan Rungger,[2] Peter Zapol,[1] and Olle Heinonen[1, 3, b)]
[1)] *Materials Science Division, Argonne National Laboratory, Lemont, Illinois 60439, USA*
[2)] *Materials Division, National Physical Laboratory, Teddington, TW11 0LW, United Kingdom*
[3)] *Northwestern-Argonne Institute for Science and Engineering, Northwestern University, 2145 Sheridan Rd., Evanston, Illinois 60208, USA*

Memristive switching devices, candidates for resistive random access memory technology, have been shown to switch off through a progression of states with quantized conductance and subsequent non-integer conductance (in terms of conductance quantum G_0). We have performed calculations based on density functional theory to model the switching process for a Pt-HfO_2-Pt structure, involving the movement of one or two oxygen atoms. Oxygen atoms moving within a conductive oxygen vacancy filament act as tunneling barriers, and partition the filament into weakly coupled quantum wells. We show that the low-bias conductance decreases exponentially when one oxygen atom moves away from interface. Our results demonstrate the high sensitivity of the device conductance to the position of oxygen atoms.

I. INTRODUCTION

Memristive switching devices are currently intensively investigated as potential candidates for non-volatile resistive random access memories because of their scalablility, low-power and high-speed features[1]. The architecture of a typical device consists of a thin film of resistive switching material sandwiched between two electrodes. Recently, quantized conductance has been observed for various resistive switching materials, e.g, AgI[2], Ag_2S[3,4], and a range of transition metal oxides including ZnO[5], HfO_2[6], TiO_2[7], Ta_2O_5[8] and V_2O_5[9]. Specifically, during the 'set' (switching from the off-state to the on-state) and/or the opposite 'reset' process, the measured conductance exhibits a sequence of states with a distribution of peaks at integer multiples (from one to a few) of the conductance quantum $G_0 = 2e^2/h$. Understanding the resistive switching phenomena is crucial towards reducing device variance, which is considered as a key challenge to bring memristive switching devices from lab to market[1]. Observations of the evolution of the conductance during set or reset processes, including conductance quantization as well as subsequent pinch-off of the conductance during reset, provide ideal opportunities to uncover the switching mechanism.

It is believed that resistive switching in HfO_2-based devices is an atomistic process involving motion of oxygen in the oxide towards the positive electrode, which creates a reduced oxide with oxygen vacancies[1,10]. Based on DFT calculations, a linear filament model of oxygen vacancy (V_o) has been proposed[11,12] for HfO_2-based devices. This filament model predicts quantized conductance consistent with experimental work[6], wherein quantized conductance is observed in Pt/HfO_2/Pt structures in the last few on-states before reaching an insulating off-state. However, knowledge of how the system switches between on-states and off-states is still lacking. In this work we use DFT-based quantum transport simulations to model the conductance evolution of a HfO_2-based device when one or two oxygen atoms move within an oxygen-vacancy rich filament during set or reset processes. Our calculations show, remarkably, that one (two) oxygen atoms effectively divides the V_o filament into two (three) potential wells with midgap states, which can be well described by one-dimensional potential well states. The conductance of the device depends very sensitively on the location of the blocking oxygen atoms and can change orders of magnitudes when a single oxygen atom moves $\lesssim$1 nm.

II. COMPUTATIONAL METHOD

Our modeling is based on DFT[13,14] as implemented in the SIESTA/Smeagol electronic structure and transport codes[15–19]. We adopt the so-called GGA+U method, which adds on-site U parameters[20] to the generalized gradient approximation (GGA) functional[21]. The values of the U-parameters used here are 8 eV for Hf 5d orbitals and 3 eV for O 2p orbitals, respectively. The U-parameters and other calculation parameters are the same as in our recent work on the TiN-Ta-HfO_2 heterostructure[22].The adopted basis set is single zeta (SZ) for O and SZ plus polarization (SZP) for Pt and Hf. The calculated lattice constants are 3.98 and 5.10 Å for Pt and HfO_2, respectively, which agree well with the experimental values[23,24] of 3.92 and 5.12 Å. The lattice constants of our supercell in the xy-plane (see Fig. 1 (a)) are 10.81 Å along the $\hat{x}$-axis, and 10.20 Å along the $\hat{y}$-axis, respectively. For geometry relaxation and transport calculations we use a 2x2x1 k-point sampling.

[a)] Electronic mail: zhongx@anl.gov
[b)] Electronic mail: heinonen@anl.gov

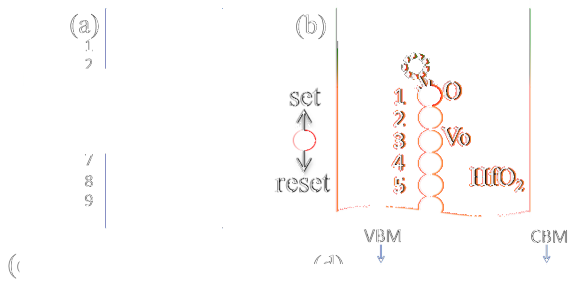

FIG. 1. (a): optimized atomic structure of Model 1 in device Set **I** (see text). Green, yellow, and pink colors represent Pt, Hf, and O atoms, respectively, with the blocking oxygen highlighted in red. The numbers in both (a) and (b) represent oxide atomic layers in the HfO_2; (b): cartoon of the modeled reset process in which a single oxygen atom moves from the top Pt electrode to block the V_o filament in the oxide film; (c): evolution of the device conductance in units of G_0 for both Set **I** and Set **II** as an oxygen atom blocks the V_o filament at different atomic layers. The dashed line (Set II*) uses a smaller energy range to estimate the conductance (see text); (d): electron transmission (T) in units of G_0 as a function of energy for selected models in Set **II**. The locations of the conduction band minimum (CBM) and the valence band maximum (VBM) of stoichiometric HfO_2 are indicated at the top of the panel. It is clear that transmission around the device Fermi level (set to zero energy) is dominated by the V_o filament.

III. RESULTS AND DISCUSSION

A. CALCULATED DEVICE CONDUCTANCE AND COMPARISON WITH EXPERIMENTS

We have modeled two sets, Set **I** and Set **II**, of a Pt-HfO_2-Pt device to include the effect of the switching material thickness on the electronic properties. Set **I** (Set **II**) is based on a structure with nine (15) cubic HfO_2 atomic layers with the total thickness of 1.6 nm (2.7 nm). Six Pt atomic layers are always included on both sides of the oxide simulating the electrodes. For both sets we first consider the case of a fully open filament by removing from each oxide layer an adjacent oxygen atom (Model 0 in Set **I** and Model 0' in Set **II**), forming a metallic oxygen vacancy (V_o) filament penetrating the entire oxide film[12,22]. For both sets we also consider the case where the filament is blocked by a single oxygen atom. We denote different atomic models by Model 1 (1'), Model 2 (2'), and so on for Set **I** (Set **II**). These models are constructed by placing a single oxygen atom at the oxide atomic layer corresponding to the index of each model [see Fig. 1 (b) for an illustration of Model 1]. Because we adopt an approximately symmetric model[25] with 9 (15) HfO_2 atomic layers in Set **I** (Set **II**), 5 (8) models are included to represent all possible independent blocked cases in Set **I** (Set **II**). We also consider representative models of two oxygen atoms blocking the filament for Set **II**, with the results for the low-bias conductance shown in Table I.

TABLE I. Low-bias conductance in units of G_0 for representative models in device Set **II** when two oxygen atoms block the conducting filament. Model 1'-2' denotes the case where one oxygen atom is located at the first oxide atomic layer and the other at the second oxide layer, and so on.

Model	1'-2'	1'-5'	1'-8'	4'-8'	7'-8'
conductance	0.053	0.011	0.37	0.014	0.00076

Figure 1 (c) depicts how the low-bias conductance evolves when one blocking oxygen atom moves inside the V_o filament. The low-bias conductance is estimated as the averaged electron transmission in an energy range from E_f-0.2 eV to E_f+0.2 eV (E_f being the Fermi energy), corresponding to read-out voltages in the range of 0.4 V, which is typical for memristors. We have also evaluated the conductance in a smaller energy range from E_f-0.1 eV to E_f+0.1 eV, corresponding to a read-out voltage in the range of 0.2 V [Figure 1 (c), dashed line], which shows the same trend of conductance variation. For both Set **I** and Set **II**, the device conductance decreases exponentially when one blocking oxygen moves from the interface to the fifth oxide layer. Figure 1 also shows that for Set **II** the conductance rather unexpectedly increases exponentially as the oxygen atoms moves from layer 5 to layer 8, which is at the midpoint of the V_o filament. The electron transmission probability[16–18], T, underlying the conductance, is also plotted in Fig. 1 (d) as a function of energy for a single blocking oxygen atom. This figure shows that T at E_f, and also in the whole spectrum where the conductance is dominated by vacancy states (from E_f-3 eV to E_f+1 eV), is rapidly reduced as the blocking oxygen atom moves towards the fifth layer from interface, and then enhanced as the oxygen moves from the fifth layer to the eighth layer. Table I shows that the conductance of a filament with two blocking oxygen atoms varies greatly (by three orders of magnitude) depending on the locations of the two atoms.

In the experimental work of Ref. 6, the low-resistance states have a large conductance of about 10^2 G_0, signaling conducting filaments with a large diameter and many conducting channels. During the reset process the conductance is at first reduced to one or a few G_0, which shows that many of the channels are pinched off and the device is entering a one-dimensional quantum regime. The transition from these intermediate conducting states to the final high-resistance states is very abrupt, with the final conductance attaining a value of about 10^{-2} G_0. Our calculated conductance for the fully open filament is

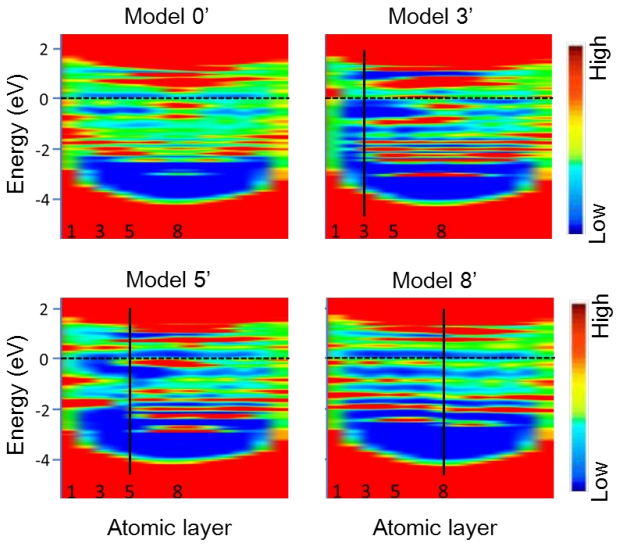

FIG. 2. Local density of states (LDOS) of the HfO_2 film sandwiched between Pt electrodes (selected models in Set **II**). The horizontal axis represents the z-axis with the numbers 1, 3, 5,...8, denoting the location of the corresponding oxide atomic layer. The vertical solid line shows the position of the blocking oxygen atom. The color maps denote the LDOS in arbitrary units. The Fermi level is set at zero energy and indicated by dotted horizontal lines.

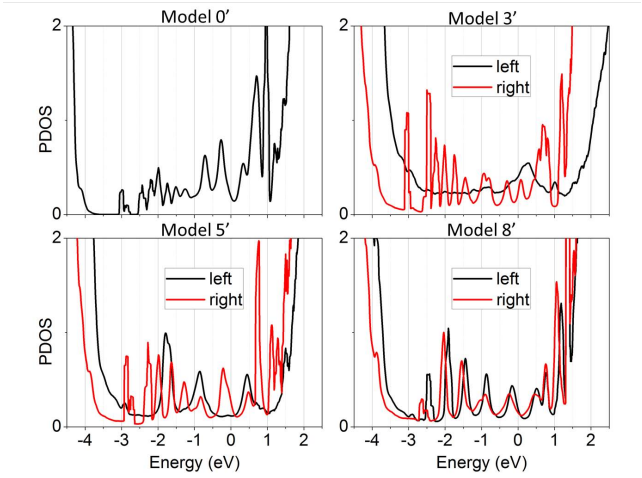

FIG. 3. Averaged PDOS of QWs (see text) for selected models. 'left' ('right') denote the averaged PDOS to the left (right) of the blocking atom. The Fermi level is set at zero energy.

1.02 and 1.13 G_0 for Model 0 and 0', respectively. This is consistent with the experimental distribution of the conductance of the intermediate states, which has a peak at G_0. When an oxygen atom moves into the filament, the conductance decreases exponentially, and with the oxygen at the fourth oxide layer, the conductance becomes two orders of magnitude smaller than that of the open V_o filament. Because the interlayer spacing between HfO_2 atomic layers is 1.8 Å, the Pt-HfO_2-Pt device is in this case effectively switched off by a single oxygen atom moving less than one nm. When a second oxygen atom moves into the filament, the conductance is in general further constrained (Table I), and in most cases the conductance ranges from 10^{-3} G_0 to 10^{-2} G_0. Therefore, the modeled filament with one or two blocking oxygen atoms can account for the experimentally observed very large resistance variation in the high-resistance states, which spans a range from 10^4 Ω to more than 10^7 Ω (or equivalently, from about 10^{-3} G_0 to G_0 in conductance).

B. CONNECTION BETWEEN DEVICE CONDUCTANCE AND ITS ELECTRONIC STRUCTURE

In order to understand the predicted features in T we now analyze the electronic structures of the modeled devices. We will focus on Set **II** as the same switching mechanism applies to both sets. Figure 2 shows the local density of states (LDOS) of the sandwiched oxide for selected models of Set **II**. The blue regions indicate negligible LDOS in the fundamental energy gap of HfO_2. The outermost oxide atomic layers exhibit finite LDOS in the full energy range as a result of hybridization of the Pt-HfO_2 states at the interface, giving rise to midgap evanescent interface states. The oxide LDOS also shows a clear band bending up to the 5th atomic layer from the Pt interface. Within the blue midgap regions there exist bright stripes, which are the midgap eigenstates in the finite length V_o filament. We note that these states have the appearance of one-dimensional (1D) quantum well (QW) states. For model 0' there is no oxygen atom blocking the filament, and these midgap eigenstates are confined by the two Pt/HfO_2 interfaces on both sides. The blocking oxygen atom divides the V_o filament into two QWs for models 3', 5' and 8' (Fig. 2). A similar analysis has been used previously to compare modeling results to experimental data to show that hydrogen atoms behave as semitransparent barriers when binding to silicon nanowires[26]. Fig. 2 also shows a strong dependence of number of QW states on QW length, with more midgap states for longer QWs.

To help analyze the nature of the midgap states and to correlate the electronic structure with transport properties, the averaged projected density of states (PDOS) is shown in Fig. 3. The average PDOS is obtained by calculating the LDOS on the left and right side of the blocking oxygen atom, respectively, and averaging over the thickness of the left and right side. Comparing Figs. 2 and 3 we note that each PDOS peak corresponds to a QW eigenstate (a bright stripe in Fig. 2). The number of QW states in the midgap region (from about -3 eV to 1 eV) is nearly linear with the QW length, which is consistent with a 1D square well model. Fits to a square well with infinitely high barriers using the free electron mass and using the well length as a fitting parameter gives a fitted well length typically a factor two larger than the actual

length. This is not unreasonable, given the deviations of the actual carrier mass from the ones of free electrons, as well as of the actual boundary conditions at the edges of each well, which are probably much softer than those of an infinite potential well.

In order to elucidate the switching mechanism, we now correlate the electronic structure (PDOS) with transmission. In bulk HfO_{2-x}, the oxygen vacancies give rise to a small DOS in the gap region because of two vacancy-induced bands[22]. When the oxide with a conducting filament without a blocking oxygen atom is sandwiched between two electrodes, there exist discrete vacancy-induced QW states instead of a dispersive band. This is seen as a number of peaks in PDOS in the midgap region (Fig. 3 Model 0'); at other energies in the gap states are evanescent from the electrode and transmission only occurs through tunneling. However, at energies in resonance with the QW states, transmission occurs through resonant tunneling, which gives rise to peaks in T (Fig. 1 d). Because of the relatively long QW and the intrinsic broadening of the QW states, PDOS is finite and pseudo-metallic in a large range of the gap region (from ~ -3 eV and up), and T is large in this range of energy. Because of a relatively large PDOS at the Fermi level, due to two large peaks at about -0.25 eV and +0.25 eV, the low-bias conductance is also large.

When the oxygen atom is introduced into the filament, it divides the filament into two QWs and acts as a semi-transparent barrier between the two QWs. The transmission probability is then the result of superimposing tunneling with resonances in the two QWs. With the oxygen atom in any of the first few layers, the PDOS on the left side of the oxygen (the short QW) is large and finite across the energy gap because all evanescent states in this energy range have a finite probability density in this short QW. To the right of the oxygen atom, the QW is long and there are a number of states, clearly visible in PDOS (Fig. 3 b). As the oxygen atom moves from the interface, the tunneling probability and PDOS to the left of the oxygen atom decay exponentially. This causes the overall exponential decay of T in the whole energy range of the energy gap, from about -3 eV to 1 V, even though there are clear peaks that arise from accidental degeneracies in the asymmetric QWs. This mechanism leads to the low-bias conductance, which is determined by T around E_f, to decrease exponentially (Fig. 1). Energy calculations show that the total energy of the device is lowest when the blocking oxygen atom is at the center of the filament, consistent with a weak coupling between degenerate QW states (see Supplemental Material). As the oxygen atom moves from layer 5 (Model 5') towards the center (Model 8'), the QWs now become more symmetric (Fig. 3 lower right panel), and the eigenstates in the two QWs become degenerate. The resonant peaks in T then grow rapidly because of resonant transport. In particular, T increases rapidly near E_f. As a consequence, the low-bias conductance increases quickly as the blocking oxygen atom moves from position 5 to the center

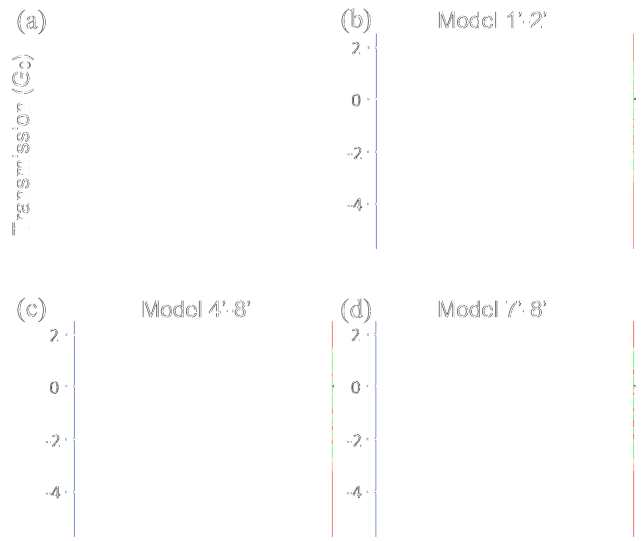

FIG. 4. (a): Transmission in units of G_0 as a function of energy for representative models in the case of two blocking oxygen atoms. (b) to (d): corresponding LDOS of the two-blocking-atom models in arbitrary unit. For all plots device Fermi level is aligned to zero energy.

(position 8). This growth gives rise to the rapid *increase* in the low-bias conductance (Fig. 1 (c)). We have also performed one calculation for a 19 oxide layers long filament and with a blocking atom at the center in order to see if the conductance saturates with device length. The low-bias conductance is calculated to be 0.35 G_0, which is quite similar to the value of 0.31 G_0 for device Set **II**. This indicates that the conductance with one oxygen atom at the V_o filament center indeed saturates as the filament length increases beyond that of Set **II** (15 atomic layers). We note a similar analysis applies to the shorter device, Set **I**.

When two oxygen atoms block the filament simultaneously device conductance is in general further suppressed (Table 1). On the other hand, there appears to be strong dependence of transmission on the locations of both atoms (Fig. 4). Transmission of Model 1'-2' is in general higher in the midgap range than that of Model 4'-8' or Model 7'-8', since in Model 1'-2' there is only one QW (Fig. 4 (b)) to the right of the two blocking atoms, and eigenstates in this QW can couple with the left electrode by evanescent interface states. The comparison between Model 4'-8' and Model 7'-8' is a little subtle. In general, transmission peaks due to resonance of QW states have similar heights for both models. The difference in low-bias conductance of about one order of magnitude (Table 1) origins from the detailed distribution of QW states in energy. For Model 4'-8' which has three QWs there are eigenstates around E_f in both the middle and the right QWs (Fig. 4 (c)). These states can couple with the left electrode by interface states, resulting in a transmission peak around E_f. For Model 7'-8' there are two QWs separated by two adjacent blocking

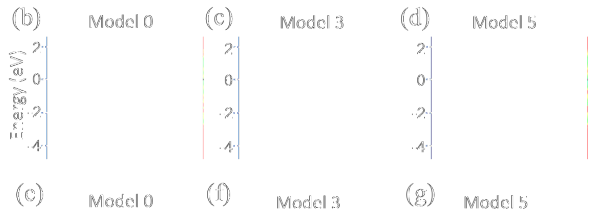

FIG. 5. (a): Electronic properties of device Set **I**. Upper: T in units of G_0 as a function of energy for selected models. Middle: LDOS of oxide in arbitrary unit. Lower: Averaged PDOS of QWs as a function of energy. For all plots the device Fermi level is aligned to zero energy.

atoms. On each side of the blocking atoms E_f locates at about the middle of two midgap states, resulting in a suppression of transmission about E_f (Fig. 4 (a)).

A similar analysis applies to the shorter device, Set **I**. Figure 5 shows transmission and electronic structures for this device. Without the oxygen atom (Model 0) each QW eigenstate spans the whole oxide thickness, leading to large peaks in T at the energies of the QW states [Fig. 5 (a)]. As the blocking atom is introduced and moves towards the center of the oxide, it divides the filament into two QWs. Because this filament is shorter than the one in Set **II**, the QW state energies and PDOS are different from those of Set **II**. In particular, with the oxygen atom at the center of the filament, there are QW energies at ~ -0.75 eV and 0.5 eV, as seen in the PDOS in Fig. 5, and a minimum in PDOS at the Fermi energy. This suppresses the low-bias conductance in this case. When two atoms block the filament simultaneously, the filament is in general divided into three QWs, except in the cases where the two atoms are located in adjacent atomic layers; this effectively results in a wider barrier and weaker coupling between the QWs.

C. ENERGIES

It is interesting to compare the energies of the different models in order to assess their relative thermodynamic stability, which is shown in Fig. 6. In each device set, total energy (E_{tot}) is defined as the energy difference between one model with blocking atoms and the model without blocking atoms (Model 0 in Set **I** and Model 0' in Set **II**). We note that because we are using a rather small basis set, the energy values should be considered semi-quantitative. Nevertheless, Fig. 6 clearly shows the trend that as one oxygen atom moves from interface towards the filament center, the total energy of the device in general decreases. Compared with structures in Set **I** which have about 350 atoms, structures in Set **II** have about 450 atoms and show a larger fluctuation in energy superimposed on the same trend. This may be due to the fact that structures in Set **II** have more degrees of freedom and may relax to different local minima. Besides, there are different quantum wells in Set **I** and Set **II**, which may also lead to different energies. As one oxygen atom moves towards the filament center, the two QWs on both sides become more symmetric, and it is expected that any weak coupling between the QW states will reduce the total energy. We also note that Pt is a noble metal that shows poor affinity for oxygen; this may also result in total energy reduction as the oxygen atom initially moves away from the electrode.

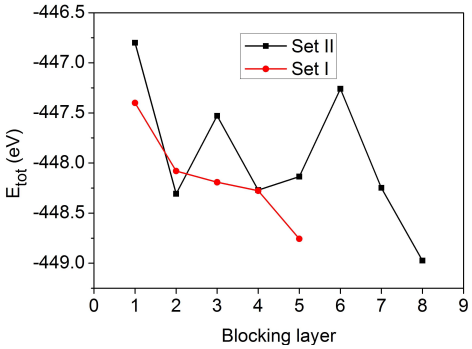

FIG. 6. Total energy (E_{tot}) variation when one oxygen atom blocks Vo filament at different locations for both device sets. E_{tot} for Model 1 and Model 1' have been aligned to zero energy.

IV. CONCLUSIONS

In summary, we have modeled the set/reset processes of memristive switching devices based on Pt-HfO_2-Pt heterostructures. It is remarkable, that blocking oxygen atoms separate the filament into weakly coupled 1D QWs. The conductance mechanism as oxygen atoms are placed in the filament is a combination of tunneling with resonances at QW energies. When a blocking oxygen atom moves into the V_o filament from the interface, the conductance first decreases exponentially because the exponential decay of midgap states away from the interface dominates the transmission. When the blocking atom moves closer towards the center of the V_o filament, T increases because of increasing alignment of QW eigenstates within the two QWs as the QWs become identical. When two oxygen atoms simultaneously block the filament, the device conductance shows a large variation

over several orders of magnitude. Our work explains the evolution of conductance observed experimentally[6], and provides a detailed atomistic mechanism for the set/reset process. Furthermore, PDOS at the Fermi energy depends sensitively on the channel length and QW lengths. Because the low-bias conductance depends on PDOS and transmission at the Fermi energy, the low-bias conductance therefore shows a high sensitivity to the oxide thickness and filament length.

ACKNOWLEDGMENTS

The work by X.Z., P.Z. and O.H. was supported by U. S. DOE, Office of Science under Contract No. DE-AC02-06CH11357. I.R. acknowledges financial support from the European Union's Horizon2020 research and innovation programme within the PETMEM project (Grant agreement number 688282). We gratefully acknowledge the computing resources provided on Blues and Fusion, high-performance computing clusters operated by the Laboratory Computing Resource Center at Argonne National Laboratory.

[1] J. J. Yang, D. B. Strukov, and D. R. Stewart, Nat. Nanotechnol. **8**, 13 (2013).
[2] S. Tappertzhofen, I. Valov, and R. Waser, Nanotechnology **23**, 145703 (2012).
[3] K. Terabe, T. Hasegawa, T. Nakayama, and M. Aono, Nature **433**, 47 (2005).
[4] J. J. Wagenaar, M. Morales-Masis, and J. M. van Ruitenbeek, Journal of Applied Physics **111**, 014302 (2012).
[5] X. Zhu, W. Su, Y. Liu, B. Hu, L. Pan, W. Lu, J. Zhang, and R.-W. Li, Advanced Materials **24**, 3941 (2012).
[6] S. Long, X. Lian, C. Cagli, X. Cartoixà, R. Rurali, E. Miranda, D. Jimnez, L. Perniola, M. Liu, and J. Su, Appl. Phys. Lett. **102**, 183505 (2013).
[7] C. Hu, M. D. McDaniel, J. G. Ekerdt, and E. T. Yu, Electron Device Letters, IEEE **34**, 1385 (2013).
[8] C. Chen, S. Gao, F. Zeng, G. Wang, S. Li, C. Song, and F. Pan, Applied Physics Letters **103**, 043510 (2013).
[9] E.-J. Yun, M. Becker, and R. Walser, Applied physics letters **63**, 2493 (1993).
[10] F. D. Stefano, M. Houssa, V. V. Afanas'ev, J. A. Kittl, M. Jurczak, and A. Stesmans, Thin Solid Films **533**, 15 (2013), {EMRS} 2012 Symposium L.
[11] X. Lian, X. Cartoixa, E. Miranda, L. Perniola, R. Rurali, S. Long, M. Liu, and J. Suñé, J. Appl. Phys. **115**, 244507 (2014).
[12] X. Cartoixà, R. Rurali, and J. Suñé, Phys. Rev. B **86**, 165445 (2012).
[13] P. Hohenberg and W. Kohn, Phys. Rev. **136**, B864 (1964).
[14] W. Kohn and L. J. Sham, Phys. Rev. **140**, A1133 (1965).
[15] J. M. Soler, E. Artacho, J. D. Gale, A. Garca, J. Junquera, P. Ordejón, and D. Sánchez-Portal, J. Phys. Condens. Matter. **14**, 2745 (2002).
[16] I. Rungger and S. Sanvito, Phys. Rev. B **78**, 035407 (2008).
[17] A. R. Rocha, V. M. Garcia-Suarez, S. W. Bailey, C. J. Lambert, J. Ferrer, and S. Sanvito, Nat. Mater. **4**, 335 (2005).
[18] A. R. Rocha, V. Garcia-Suarez, S. Bailey, C. Lambert, J. Ferrer, and S. Sanvito, Phys. Rev. B **73**, 085414 (2006).
[19] C. D. Pemmaraju, T. Archer, D. Sánchez-Portal, and S. Sanvito, Phys. Rev. B **75**, 045101 (2007).
[20] M. T. Czyżyk and G. A. Sawatzky, Phys. Rev. B **49**, 14211 (1994).
[21] J. P. Perdew, K. Burke, and Y. Wang, Phys. Rev. B **54**, 16533 (1996).
[22] X. Zhong, I. Rungger, P. Zapol, H. Nakamura, Y. Asai, and O. Heinonen, Phys. Chem. Chem. Phys. **18**, 7502.
[23] J. W. Edwards, R. Speiser, and H. L. Johnston, J. Appl. Phys. **22**, 424 (1951).
[24] L. Passerini, Gazz. chim. ital **60**, 762 (1930).
[25] We note that the filament model is not exactly symmetric because of different oxide terminations at the two Pt interfaces. This will result in a very slight asymmetry in properties such as projected density of states near the interfaces.
[26] B. Naydenov, I. Rungger, M. Mantega, S. Sanvito, and J. J. Boland, Nano letters **15**, 2881 (2015).